Eur Biophys J (2010) 39:993–999
DOI 10.1007/s00249-009-0470-9

ORIGINAL PAPER

Compartmentalization of the redox environment in PC-12 neuronal cells

G. Maulucci · G. Pani · S. Fusco · M. Papi · G. Arcovito · T. Galeotti · M. Fraziano · M. De Spirito

Received: 14 February 2009 / Revised: 20 April 2009 / Accepted: 29 April 2009 / Published online: 3 June 2009
© European Biophysical Societies' Association 2009

Abstract Neuronal redox phenomena are involved in numerous biochemical pathways and play a key role in many pathological events and clinical situations. The oxidation/reduction (redox) state present in biological compartments is a major target for possible pharmaceutical intervention and, consequently, the processes associated with its change have attracted increased attention in recent years. Here, we analyze the redox environment and its spatial compartmentalization in differentiated neuronal phenotype of PC-12 cells using a redox-sensitive protein (i.e., a mutant of the Yellow Fluorescent protein), employed ratiometrically. Redox maps of cells were generated with an elevate spatial resolution, and the spatial distributions of highly oxidized and highly reduced regions have been determined. A quantitative analysis of redox maps allows the disclosure of a peculiar spatial organization of the redox environment.

Keywords ROS · Neuron · Redox environment · rxYFP · Compartmentalization

Proceedings of the XIX Congress of the Italian Society of Pure and Applied Biophysics (SIBPA), Rome, September 2008.

G. Maulucci · M. Papi · G. Arcovito · M. De Spirito (✉)
Istituto di Fisica, Università Cattolica del Sacro Cuore, L.go Francesco Vito 1, 00168 Rome, Italy
e-mail: m.despirito@rm.unicatt.it

G. Pani · S. Fusco · T. Galeotti
Istituto di Patologia Generale, Università Cattolica del Sacro Cuore, L.go Francesco Vito 1, 00168 Rome, Italy

M. Fraziano
Dipartmento di Biologia, Università di Roma "Tor Vergata", Via della Ricerca Scientifica, 00133 Rome, Italy

Introduction

Reactive oxygen species (ROS), such as superoxide (O_2^-) and hydrogen peroxide (H_2O_2), are produced intracellularly as part of normal metabolic reactions (Babior 2002; Vignais 2002). ROS are very reactive oxidants (Liochev 1996; Turrens 2003) and their excessive, uncontrolled production can have detrimental effects on cellular physiology and function, often leading to apoptosis and to a variety of diseases (Finkel 2003).

Recent studies have suggested that elevated, but sublethal, levels of (O_2^-) and H_2O_2 can act to influence intracellular signaling pathways in cells by modulating gene expression, cellular growth, and differentiation (Droge 2002; Finkel 1998; Hancock et al. 2001; Kamata and Hirata 1999; Klann and Thiels 1999; Rhee 1999).

ROS have been shown to be essential for the NGF-induced differentiation of PC-12 cells (Katoh et al. 1997, 1999; Suzukawa et al. 2000) and, in hippocampal neurons, high levels of O_2^- (Bindokas et al. 1996) modulate neuronal plasticity (Hongpaisan et al. 2004). Redox state has also been shown to modulate differentiation of mesencephalic precursors (Lee et al. 2003) and of neural crest stem cells (Morrison et al. 2000). ROS can therefore influence multiple aspects of neural differentiation and function, including the survival and the plasticity of neurons, the proliferation of neural precursors, as well as their differentiation into specific neuronal cell types. The determination of induced variations in redox environment by ROS at high spatial resolution is therefore crucial, and could promote novel therapeutic approaches aimed at protecting against oxidative stress by identifying specific redox-sensitive sites that could then be targeted for intervention.

Whilst traditional biochemical analysis of tissue and cell extracts suffer from several technical limitations when

seeking to determine the redox environment, fluorescence ratio imaging microscopy allows one to determine intracellular redox state by making it possible to cancel out most or all of the potential variability caused by instrument efficiency and effective dye content (Bright et al. 1987; Bizzarri et al. 2006; Gross et al. 1994; Luby-Phelps et al. 1993; Dooley et al. 2004).

A redox-sensitive variant of the Yellow Fluorescent Protein (rxYFP) (Ostergaard et al. 2001, 2004) has been successfully employed ratiometrically to measure the fraction R of reduced rxYFP at equilibrium (Maulucci et al. 2008; Koch et al. 2008)

$$R = \frac{[rxYFP_{\mathrm{red}}]}{[rxYFP_{\mathrm{ox}}] + [rxYFP_{\mathrm{red}}]} \tag{1}$$

where $[rxYFP_{\mathrm{red}}]$, $[rxYFP_{\mathrm{ox}}]$ are respectively the concentrations of the reduced and oxidized forms of the protein. R, therefore, can monitor any oxidative/reductive state of the protein, independent of possible experimental artifacts (dye concentration, photobleaching, intensity fluctuations, etc.). By mapping R over the whole microscope scanning field, images representative of the sample redox status, at a resolution of 200 nm (the minimum confocal voxel size), can be created (Maulucci et al. 2008). Redox maps allow the visualization and characterization of the spatial compartmentalization of cellular oxido-reductive reactions, which provides a powerful mechanism for controlling numerous biological processes and signaling events that have to be adjusted rapidly in response to environmental or physiological changes (Pani et al. 2001; Finkel 2003). Here, we analyze the redox environment and its spatial compartmentalization in PC-12 neuronal cells using R-based pseudoimages. High spatial resolution redox maps were generated, and the spatial distributions of highly oxidized and highly reduced regions have been determined. Histograms of redox maps permit the disclosure of a peculiar organization of the redox environment.

Materials and methods

Plasmids and cell lines

The cDNA encoding for rxYFP was obtained from Dr. J. R. Winther (Carlsberg Laboratories, Copenhagen, Denmark) and subcloned in the unique EcorI site of the mammalian expression vector pCDNA3 (Invitrogen, San Giuliano Milanese, Italy). The PC-12 rat pheochromocytoma neuronal cell line was obtained from the American Type Culture Collection (ATCC) and differentiated with Nerve Growth Factor (100 ng/ml for 2 weeks). Cell lines are routinely maintained in Dulbecco's Modified Eagle's Medium (DMEM) supplemented with pyruvate, glutamine, antibiotics, non-essential aminoacids and 8% v/v fetal calf serum, all from BioWest (Nuaille', France). Cell transfection was performed in glass-bottomed 30-mm tissue culture dishes (Ibidi, Integrated Biodiagnostic, Martinsried, Germany) with lipofectamine 2000 reagent (Invitrogen), according to the manufacturer's recommendations. Expression of transgenes was verified using fluorescent microscopy (rxYFP).

Confocal microscopy

Images were obtained by using an inverted confocal microscope (DMIRE2; Leica Microsystems, Germany) fitted with a 63× oil immersion objective (NA 1.4) and LCS 2.61 acquisition Software (Leica Microsystems). Internal photon multiplier tubes collected 8-bit, unsigned images at a 400-Hz scan speed. rxYFP was excited by two argon-ion laser lines (excitation wavelength: 458 and 488 nm; emission range: 530–600 nm). 3D reconstructions, x–z sections and analysis of images acquired were performed with IMAGEJ 1.41 (NIH).

Redox map generation

The fraction R of reduced rxYFP ($rxYFP_{\mathrm{red}}$) at equilibrium (Eq. 1) can be related to easily measurable experimental quantities: fluorescence emission of rxYFP when excited at 488 nm (F_{488}) and fluorescence emission when excited at 458 nm (F_{458}) (Maulucci et al. 2008). Indeed, by assuming that probe concentration and path length are small enough, the fluorescence contributions from the reduced ($rxYFP_{\mathrm{red}}$) and oxidized ($rxYFP_{\mathrm{ox}}$) forms are proportional to their concentration $[rxYFP_{\mathrm{red}}]$, $[rxYFP_{\mathrm{ox}}]$, and the total fluorescence intensities at wavelengths λ is

$$F = \epsilon^{\lambda}_{\mathrm{red}}[rxYFP_{\mathrm{red}}] + \epsilon^{\lambda}_{\mathrm{ox}}[rxYFP_{\mathrm{ox}}] \tag{2}$$

where $\epsilon^{\lambda}_{\mathrm{red}}$ and $\epsilon^{\lambda}_{\mathrm{ox}}$ are factors accounting for the excitation intensity, extinction coefficient, path length, quantum efficiency, and the instrumental efficiency in collecting emitted photons from reduced and oxidized rxYFP, respectively, at a wavelength λ. The ratio of the total fluorescence intensities measured at wavelengths λ_{488} and λ_{458}, by using Eq. (2) becomes:

$$F = \frac{\epsilon^{\lambda_{488}}_{\mathrm{red}}[rxYFP_{\mathrm{red}}] + \epsilon^{\lambda_{488}}_{\mathrm{ox}}[rxYFP_{\mathrm{ox}}]}{\epsilon^{\lambda_{458}}_{\mathrm{red}}[rxYFP_{\mathrm{red}}] + \epsilon^{\lambda_{458}}_{\mathrm{ox}}[rxYFP_{\mathrm{ox}}]} \tag{3}$$

where $F_{\mathrm{ox}} = \epsilon^{\lambda_{488}}_{\mathrm{ox}}/\epsilon^{\lambda_{458}}_{\mathrm{ox}}$ and $F_{\mathrm{red}} = \epsilon^{\lambda_{488}}_{\mathrm{red}}/\epsilon^{\lambda_{458}}_{\mathrm{red}}$ are the ratios of the completely reduced and oxidized protein, respectively. By combining Eqs. (1) and (3), we obtain

$$R = \frac{a(F - F_{\mathrm{ox}})}{F_{\mathrm{red}} - aF_{\mathrm{ox}} + F(a-1)} \tag{4}$$

where $a = \epsilon_{ox}^{\lambda_{458}}/\epsilon_{red}^{\lambda_{458}}$ is a probe-specific factor describing residual redox sensitivity at the reference excitation wavelength. It should be noted that at an entirely redox-insensitive wavelength (i.e., corresponding to an isosbestic point) $a = 1$. In this case, Eq. 4 reduces to an even simpler expression $R = (F - F_{ox})/(F_{red} - F_{ox})$. The fraction R of reduced rxYFP at equilibrium, therefore, can be easily determined by measuring experimentally accessible quantities (F_{488}, F_{458}, F_{ox}, F_{red}, a) (Maulucci et al. 2008). By mapping R over the entire microscope scanning field, images representative of the phoenix cell redox status, at a resolution of 200 nm (the minimum confocal voxel size), are created (Fig. 1a). Redox maps were generated with the software Redox Maps Generator 1.0 (Maulucci et al. 2008).

Statistics

To ensure significant variations of R values, R-histograms were determined within multiple regions of interest (single cells) for each sample, and their mean ± SD (n = 15) determined and utilized for further statistical analysis (two-tailed Student's t test; OpenOffice calc).

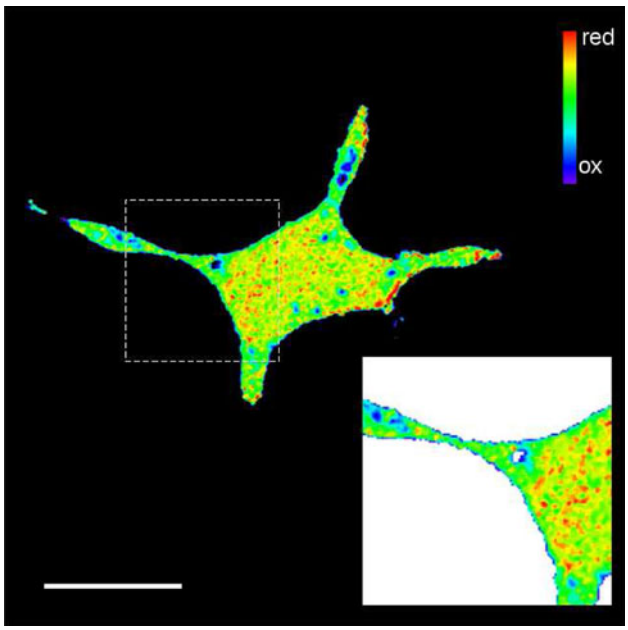

Fig. 1 Map of the PC-12 redox status, at a resolution of 240 nm. *Scale bar* 20 μm. The fraction of reduced protein R is visualized by using the lut "rainbow" that ranges from *violet* (fully oxidized protein) to *green* (50% of reduced protein) and finally to *red* (fully reduced protein). In the *inset*, an enlargement of a part of the cell is imaged on a white background. Oxidation of rxYFP occurs prevalently in the intracellular side of the plasma membrane, as evidenced by the *blue contour* of the cell, and in several, isolated spots concentrated inside neurites and along the soma borders. The cell interior, markedly *green*, shows, instead, a more reduced environment, with bright red spots that highlight highly reduced areas

Results and discussion

We report in Fig. 1a a representative image of the spatial distribution of the fraction of reduced rxYFP inside a PC-12 neuronal cell, at a spatial resolution of 240 nm. The index R is visualized by using the lut "rainbow" that ranges from violet (fully oxidized protein) to green (50% of reduced protein) and finally to red (fully reduced protein). Oxidation of rxYFP occurs predominantly in the intracellular side of the plasma membrane, as evidenced by the cyan contour of the cell (see inset of Fig. 1 where a white background has been adopted). Furthermore, oxidation occurs in several, isolated spots concentrated inside neurites and along the border of the soma. Conversely, the cell interior, which is markedly green, indicates a more reduced

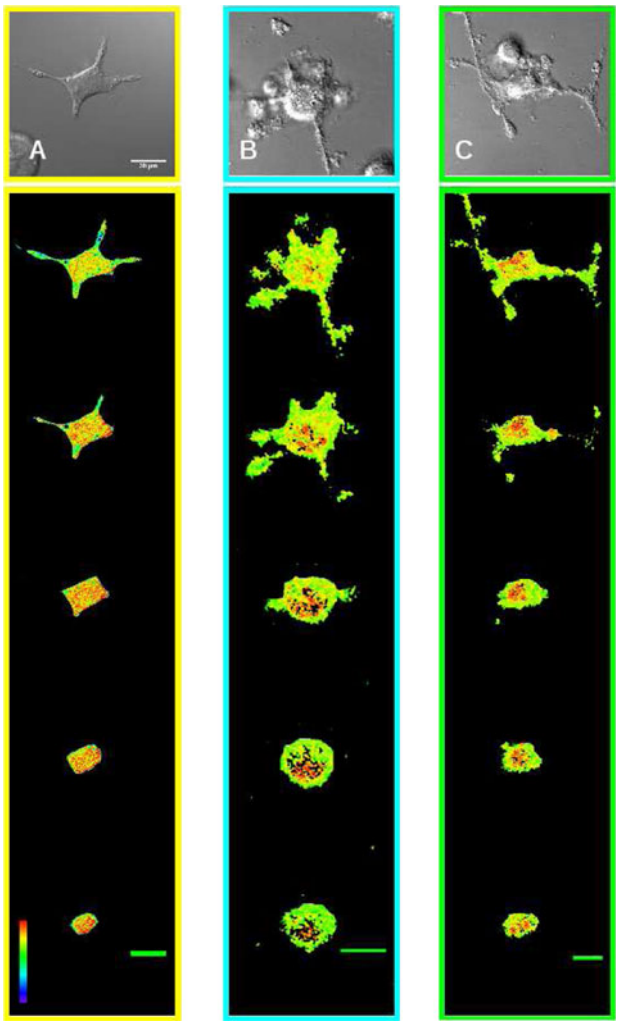

Fig. 2 Redox maps of different sections of several neurons (**a**, **b**, **c**) along the z-axis. The fraction of reduced protein R is visualized by using the lut "rainbow" that ranges from *violet* (fully oxidized protein) to *green* (50% of reduced protein) and finally to *red* (fully reduced protein). *Scale bar* 20 μm. Bright field images are also reported. All cells investigated show a similar behavior

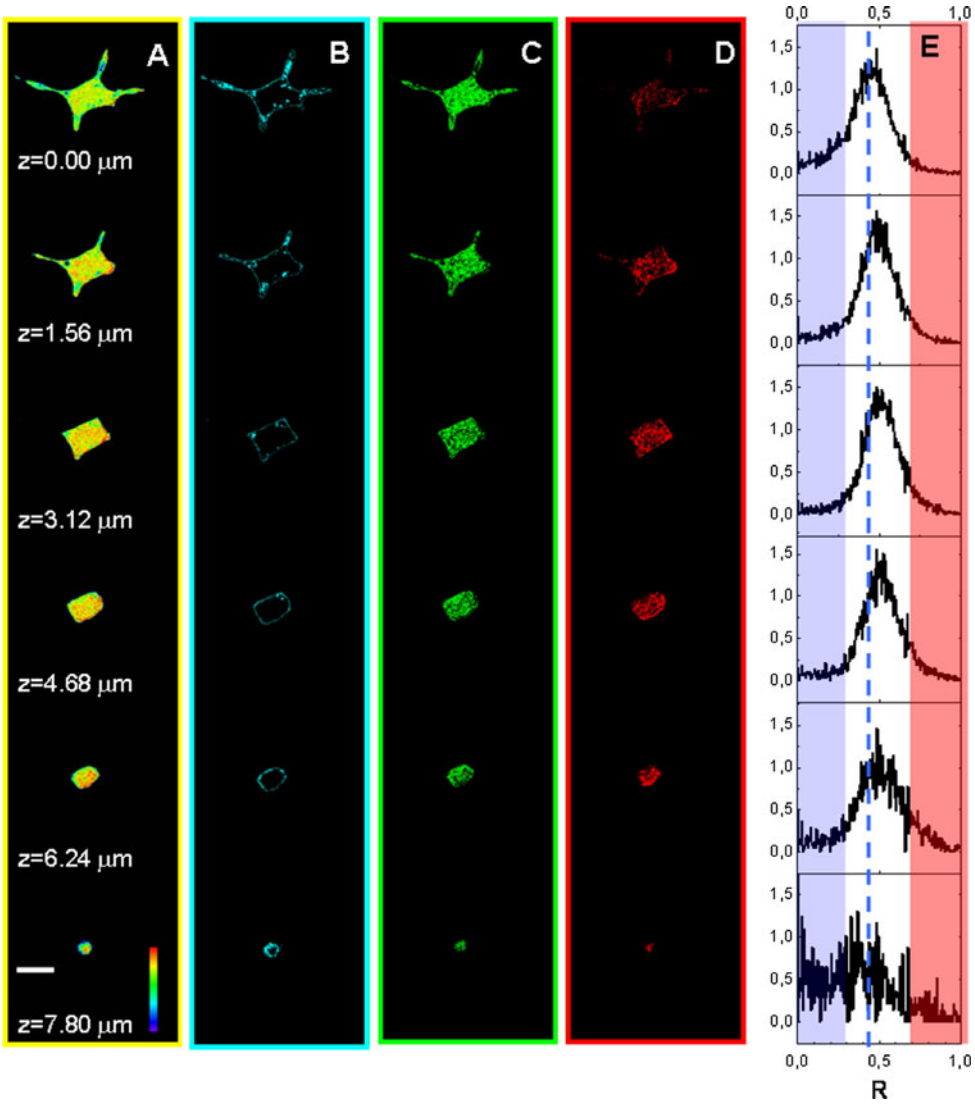

Fig. 3 **a** Redox maps of different sections of the neuron along the z-axis. Lut and scale are those of Fig. 2. *Scale bar* 20 μm. **b** Spatial distribution of oxidized voxels ($0 < R < 0.35$). Oxidized spots displays a pronounced localization on the cell contour and on isolated spots concentrated inside neurites and along the soma borders. **c** Spatial distribution of voxels that fall in th range $0.35 < R < 0.6$. The intermediate region cover homogeneously the sections of the cell. **d** Spatial distribution of reduced voxels ($0.6 < R < 1$). Reduced elements are localized in well separated spots heterogeneously distributed in the inner part of the cell. **e** R histograms of each section. An overall shift of histograms towards a more reduced state, while increasing z, occurs. The *dashed line* helps to visualize this shift. The R-histogram reflects this behavior showing a decrease in the *left part* ($0 < R < 0.35$, *violet box*). The reduced region shows a behavior completely specular to the oxidized one ($0.6 < R < 1$, *red box*)

environment, with bright red spots that highlight reduced areas.

In order to furnish a detailed three-dimensional characterization of the redox environment of PC-12 neuronal cells, redox maps of different sections of several neurons, obtained by moving the focal plane along the z-axis (i.e., from the bottom towards the apical part of the cell), were generated (Fig. 2). Bright field images are also reported.

To detail changes in the spatial distribution between the oxidized and reduced voxels, that occur while moving the focal plane, we report, for each selected z plane, three complementary regions from a single cell: an oxidized one ($0 < R < 0.35$), an intermediate one ($0.35 < R < 0.6$), and a reduced one ($0.6 < R < 1$), reported in Fig. 3, columns B, C and D, respectively.

The choice for the thresholds of the three regions arise from the analysis of the histogram of the R-image (i.e. the normalized number ($N(r)$) of pixels with a specific R value) (Fig. 3e, $z = 0$ μm). Indeed the histogram's shape, highly peaked in the central region with two lateral shoulders, reflects the peculiar spatial organization of the redox environment and allows to roughly separate oxidized and reduced voxels.

The peculiar spatial distribution of R, observed in Fig. 1 maintains its characteristics in any of the z sections examined: oxidized redox elements (Fig. 3b) display a pronounced localization on the cell contour, on isolated spots concentrated inside the neurites, and along the border of the soma, while reduced elements (Fig. 3d) are localized in well-separated spots heterogeneously distributed in the inner part of the cell. Nevertheless, differences among z-sections can be observed in R-histograms (Fig. 3e) where an overall shift of histograms towards a more reduced state, while increasing z, is observable. The mean R value, recovered from each histogram and averaged over several cells ($n = 15$), is reported in Fig. 4a, together with their

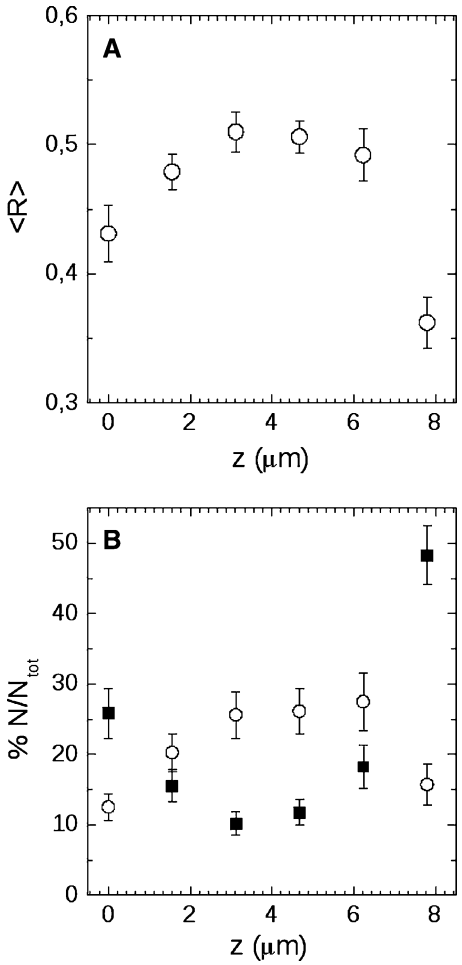

Fig. 4 **a** The averaged (over $n = 15$ cells) mean value of *R*-histogram and the relative SD are reported against the section height. In the first 3μm, the fraction of reduced rxYFP increases from 43 to 51%. After that, the mean value starts slowly to decrease up to the border of the cell where it falls abruptly to 35%, being the cells' highly oxidized border. **b** Averaged percentage of the cell section covered by oxidized voxels (*full squares*) and reduced voxels (*open circles*)

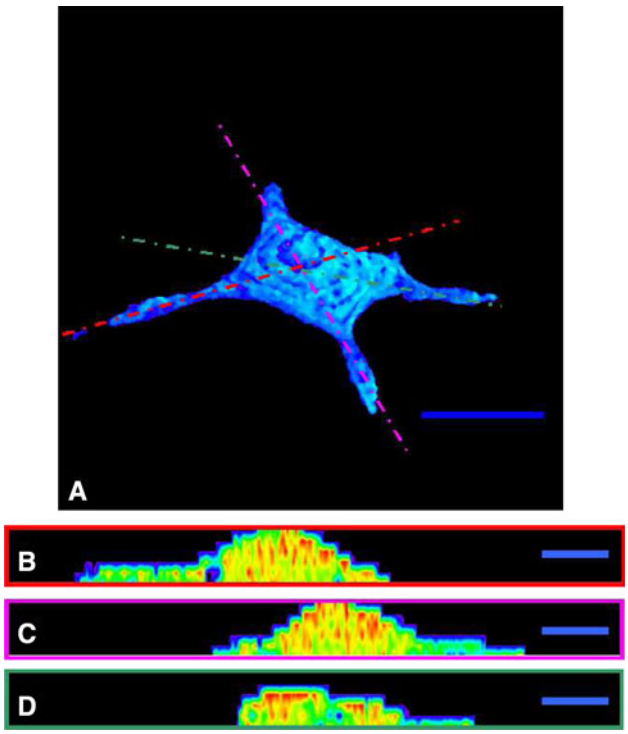

Fig. 5 **a** Three-dimensional reconstruction of the redox environment of the neuron, together with three different *x*–*z* sections (panels **b**, **c**, **d**, corresponding respectively to the *red*, *purple* and *green dashed lines*), which clearly show the compartmentalization along the *z*-axis. *Scale bar* 20 μm

standard deviation (SD), against the section height. As can be observed, in the first 3μm, the fraction of reduced rxYFP increases from 43 to 51%. After that, the mean value starts to slowly decrease up to the border of the cell, where it falls abruptly to 35%, being the cells' highly oxidized border. A simple look at the oxidized region (Fig. 3b) shows that, while increasing *z*, the number of voxels decrease in number. The *R*-histogram reflects this behavior showing a decrease in its left part (Fig. 3e, violet box). The histogram's area, calculated in the range $0 < R < 0.35$, represents the average percentage of the cell section covered by oxidized voxels (Fig. 4b, full squares). A decrease down to a minimum, at about 3 μm, can be observed. When the apical part of the cell is reached, the percentage of oxidized voxels undergoes an abrupt increase, because of the strong oxidation of the cell border. The reduced region shows a behavior completely specular to the oxidized ones (Fig. 3d). The histogram's area, calculated in the range $0.6 < R < 1$ (Fig. 4b, open circles), increases from 12 to 28%. When the apical part of the cell is reached, the percentage of reduced voxels undergoes an abrupt decrease down to 15%, because of the strong oxidation of the cell border. The percentage of the cell section covered by intermediate voxels ($0.35 < R < 0.6$) is nearly constant ($\sim$45%), with the exception of the border on the apical part of the cell ($\sim$27%).

Neuronal redox phenomena are involved in numerous biochemical pathways and play a key role in many pathological events and clinical situations. The redox state present in biological compartments is a major target for possible pharmaceutical intervention and, consequently, the processes associated with these changes have attracted increased attention in recent years. Evaluating the concentration and the compartmentalization of redox active compounds is therefore a key target to be pursued for diagnosis and treatment (Pani et al. 2001). In this context, by taking advantage of a redox-sensitive mutant of the rxYFP, employed ratiometrically, we investigated the redox environment and its spatial compartmentalization in PC-12 neuronal cells. The analysis of high spatial

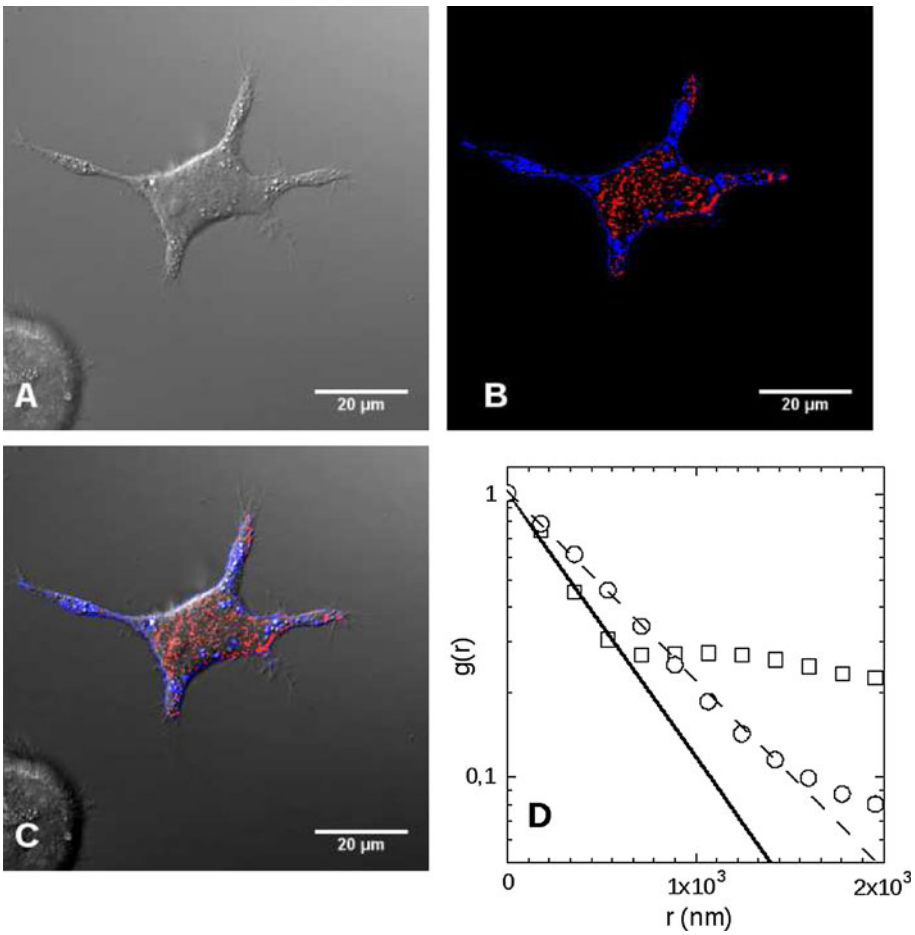

Fig. 6 **a** Bright field image of the Pc-12 cell. *Scale bar* 20 µm. **b** Spatial distribution of oxidized voxels ($0 < R < 0.35$, *blue spots*) and reduced voxels ($0.6 < R < 1$, *red spots*). **c** Overlap of (**a**) and (**b**) evidence that oxidized spots perfectly colocalize with spheroidal cellular structures. **d** Image auto-correlation functions ($g(r)$) averaged over several regions of interest (ROIs) of images in Fig. 3b (*open circles*) and in Fig. 3d (*open square*). *Dashed* and *continuous* lines represent exponential fits to experimental data. The mean dimensions of the oxidized spots ($d_{ox} \sim 640$ nm) appear to be slightly larger than those of reduced spots ($d_{red} \sim 460$ nm)

resolution redox maps allowed the disclosure of a peculiar organization of the redox environment: reduced and oxidized areas are localized in well-defined spots. While reduced spots increase in number when moving from the bottom towards the apical part of the cell, oxidized spots tend to localize on the base of the neuron, preferentially inside neurites and along the soma borders. A three-dimensional reconstruction of the redox environment of the neuron is represented in Fig. 5a, together with three different x–z sections (Fig. 5b–d) which clearly show the compartmentalization and spatial organization along the z-axis.

The mean dimensions of reduced and oxidized spots can be estimated by a specific image analysis technique called Image Correlation Spectroscopy (ICS) (Wiseman et al. 2000), which allows the determination of the 2-D pixels auto-correlation function $g(r) = \langle I_F(x,y) I_F(x+\eta, y+\xi)\rangle / \langle I_F(x,y)\rangle^2$ where $I_F(x,y)$ is the fluorescence intensity of the pixels identified by its spatial coordinates x and y, η and ξ are discrete numbers that represents the spatial step, $r = (\eta^2 + \xi^2)^{1/2}$, and the symbol $\langle\ \rangle$ represents the average over all the products.

In Fig. 6 are reported image auto-correlation functions averaged over several regions of interest (ROIs) of images in Fig. 3b (open circles) and in Fig.3d (open squares). By adopting an exponential model (Cressie 1991) to fit experimental data (dashed and continuous lines), the mean dimensions of the oxidized spots ($d_{ox} \sim 640$ nm) appear to be slightly larger than that of reduced one ($d_{red} \sim 460$ nm). Interestingly, the overlap of the bright field image with the redox map evidence that oxidized spots perfectly colocalize with spheroidal cellular structures (Fig. 6c). This evidence clearly suggests that specific cellular structures possess a distinct redox environment.

In conclusion, the analysis of three-dimensional redox stacks allowed the disclosure of a compartmentalized organization of the redox environment. Oxidized and reduced compartments, which can be fully characterized by determining their 3-D spatial position, size and density, can be a useful tool in kinetic phenomena. Indeed, changes in the compartment characteristics, in response to oxidative stress or signaling events, allow the monitoring of multiple aspects of neural differentiation and function, such as the survival and the plasticity of neurons, the proliferation of neural precursors, as well as their differentiation into specific neuronal cell types.

References

Babior B (2002) The leukocyte nadph oxidase. Isr Med Assoc J 4:1023–1024

Bindokas VP, Jordan J, Lee CC, Miller RJ (1996) Superoxide production in rat hippocampal neurons: selective imaging with hydroethidine. J Neurosci 16:1324–1336

Bizzarri R, Arcangeli C, Arosio D, Ricci F, Faraci P, Cardarelli F, Beltram F (2006) Development of a novel gfp-based ratiometric excitation and emission ph indicator for intracellular studies. Biophys J 90:3300–3314

Bright GR, Fisher GW, Rogowska J, Taylor DL (1987) Fluorescence ratio imaging microscopy: temporal and spatial measurements of cytoplasmic pH. J Cell Biol 104:1019–1033

Cressie NA (1991) Statistics for spatial data. Wiley, New York

Dooley CT, Dore TM, Hanson GT, Jackson WC, Remington SJ, Tsien RY (2004) Imaging dinamic redox changes in mammalian cells with green fluorescent proteins indicators. J Biol Chem 279:22284–22293

Droge W (2002) Free radicals in the physiological control of cell function. Physiol Rev 82:47–95

Finkel T (1998) Oxygen radicals and signaling. Curr Opin Cell Biol 10:248–253

Finkel T (2003) Oxidant signals and oxidative stress. Curr Opin Cell Biol 15:247–254

Gross E Jr, RSB, Loew LM (1994) Dual-wavelength ratiometric fluorescence measurement of the membrane dipole potential. Biophys J 67(1):208–216

Hancock JT, Desikan R, Neill SJ (2001) Role of reactive oxygen species in cell signalling pathways. Biochem Soc Trans 29:345–350

Hongpaisan J, Winters CA, Andrews SB (2004) Strong calcium entry activates mitochondrial superoxide generation, upregulating kinase signaling in hippocampal neurons. J Neurosci 24:10878–10887

Kamata H, Hirata H (1999) Redox regulation of cellular signalling. Cell Signal 11:1–14

Katoh S, Mitsui Y, Kitani K, Suzuki T (1997) Hyperoxia induces the differentiated neuronal phenotype of pc12 cells by producing eactive oxygen species. Biochem Biophys Res Commun 241:347–351

Katoh S, Mitsui Y, Kitani K, Suzuki T (1999) Hyperoxia induces the neuronal differentiated phenotype of pc12 cells via a sustained activity of mitogen-activated protein kinase induced by bcl-2. Biochem J 338:465–470

Klann E, Thiels E (1999) Modulation of protein kinases and protein phosphatases by reactive oxygen species: implications for hippocampal synaptic plasticity. Prog Neuro-Psychopharmacol Biol Psychiatr 23:359–376

Koch O, Fusco S, Ranieri SC, Maulucci G, Palozza P, Larocca LM, Farre S, Galeotti T, Spirito MD, Pani G (2008) Role of the life span determinant p66shca in ethanol-induced liver damage. Lab Invest 88:750–760

Lee JY, Chang MY, Park CH, Kim HY, Kim JHH, Son YS, Lee SH (2003) Ascorbate-induced differentiation of embryonic cortical precursors into neurons and astrocytes. J Neurosci Res 73:156–165

Liochev SL (1996) The role of iron-sulfur clusters in in-vivo hidroxyl radical production. Free Radic Res 25:369–384

Luby-Phelps K, Mujumdar S, Mujumdar RB, Ernst LA, Galbraith W, Waggoner AS (1993) A novel fluorescence ratiometric method confirms the low solvent viscosity of the cytoplasm. Biophys J 65(1):236–242

Maulucci G, Labate V, Mele M, Panieri E, Arcovito G, Galeotti T, Ostergaard H, Winther JR, Spirito MD, Pani G et al (2008) High-resolution imaging of redox signaling in live cells through an oxidation-sensitive yellow fluorescent protein. Sci Signal 1(pl3)

Morrison SJ, Csete M, Groves AK, Melega W, Wold B, Anderson DJ (2000) Culture in reduced levels of oxygen promotes clonogenic sympathoadrenal differentiation by isolated neural crest stem cells. J Neurosci 20:7370–7376

Ostergaard H, Henriksen A, Hansen FG, Winther JR (2001) Shedding light on disulfide bond formation: Engineering a redox switch in green fluorescent protein. EMBO J 20:5853–5862

Ostergaard H, Tachibana C, Winther JR (2004) Monitoring disulfide bond formation in the eukaryotic cytosol. J Cell Biol 166(3):337–345

Pani G, Bedogni B, Colavitti R, Anzevino R, Borrello S, Galeotti T (2001) Cell compartmentalization in redox signaling. IUBMB Life 52:7–16

Rhee (1999) Redox signaling: hydrogen peroxide as intracellular messenger. Exp Mol Med 31:53–59

Suzukawa K, Miura K, Mitsushita J, Resau J, Hirose K, Crystal R, Kamata T (2000) Nerve growth factor-induced neuronal differentiation requires generation of rac1-regulated reactive oxygen species. J Biol Chem 275:13175–13178

Turrens JF (2003) Mitochondrial formation of reactive oxygen species. J Physiol 552:335–344

Vignais PV (2002) The superoxide-generating nadph oxidase:structural aspects and activation mechanisms. Cell Mol Life Sci 59:1428–1459

Wiseman P, Squier J, Ellisman M, Wilson KR (2000) Two-photon image correlation spectroscopy and image cross-correlation spectroscopy. J Microsc 200(1):14–25